Photo-oxidation of Polystyrene/Clay Nanocomposites Under Accelerated UV Exposure: Effect on the Structure and Molecular Weight

Chérifa Remili,[1] Mustapha Kaci,[1] Souad Kachbi,[1] Stéphane Bruzaud,[2] Yves Grohens[2]

[1]*Laboratoire des Matériaux Organiques, Faculté de la Technologie, Université Abderrahmane Mira, Bejaia 06000, Algeria*
[2]*Laboratoire Polymères, Propriétés aux Interfaces et Composites, Université de Bretagne Sud, Rue de Saint Maudé, Lorient Cedex 56321, France*

Received 10 April 2008; accepted 24 November 2008
DOI 10.1002/app.29806
Published online 24 February 2009 in Wiley InterScience (www.interscience.wiley.com).

ABSTRACT: The present work investigates the effects of photo-oxidation under accelerated UV conditions on the structure, the molecular weight and the morphology of polystyrene (PS)/organophilic montmorillonite (OMMT) at various clay contents: 2.5, 5, and 7 wt %. Fourier transform infrared spectroscopy, viscosimetry and scanning electron microscopy were used to evaluate the extent of degradation of nanocomposite samples in comparison with neat PS, up to 216 h of exposure. The study has shown that the formation rates of both carbonyl and hydroperoxide groups increase with exposure time, being much higher for PS/OMMT nanocomposites. Moreover, it is also observed that all samples exhibit a large increase in the scission index, however less pronounced for neat PS. These results clearly indicate the formation of low molecular weight products that could arise from chain scission. Further, the photo-oxidation rate seems to be more affected by the presence of clay, which acts as a catalyst, rather than by the variation of clay contents. Finally, the degraded materials exhibit eroded surface. © 2009 Wiley Periodicals, Inc. J Appl Polym Sci 112: 2868–2875, 2009

Key words: polystyrene; clay; nanocomposites; UV test; photo-oxidation

INTRODUCTION

Polymer/layered silicate nanocomposites have drawn research attention over the last decade. Numerous articles and patent applications have been published on the subject, and a concise survey has recently been given.[1,2] The major reason is that, as it has been demonstrated, layered silicate filled polymer nanocomposites often exhibit remarkable improvement of mechanical, thermal, and physicochemical properties when compared with pure polymer and their conventional microcomposites, even at very low filler concentration due to the nano-level interactions with the polymer matrix.[3] However, additional to the achievement of such properties, the durability under specific conditions of use (outdoor exposure, γ-ray, etc.) should be strongly considered as it is an important prerequisite for a nanocomposite to find potential applications.[4] In fact, environmental durability is a key feature for polymer-clay nanocomposites in their processing and usage due to their degradation.[5] Among the various factors influencing the degradation, photo-oxidation is one of the major process which leads to discoloration, loss of mechanical properties, and embrittlement.[5–7] However, only few articles deal with photodegradation of polymer/clay nanocomposites.[3] The literature reported that the photodegradation mechanism of the polymeric matrix was not modified by the fillers, but a dramatic influence of the clay on the degradation rate was found that was attributed to interactions with antioxidants.[4] Recently, the degradability of a large number of polymer nanocomposite systems has been the object of many studies; a great deal of attention has also been focused on polystyrene (PS) clay nanocomposites.[8,9] PS is a commodity polymer that is used in a number of commercial products. It can be found in various industrial applications such as disposable food service wares, electronic product cases and protective packaging materials.[10] The objective of this article was to investigate the changes in the chemical structure and molecular weight M_w of PS/organophilic montmorillonite (OMMT) clay nanocomposite films subjected to photo-oxidation under accelerated UV test. The effect of the organophilic clay content on both the photo-oxidation rate and the molecular mass evolution was also considered. The results obtained have been discussed on the basis of neat polymer. Besides this, the structural characterization by wide angle X-ray scattering (WAXS), rheological measurements and thermal properties of PS/OMMT nanocomposites with various clay contents (2.5, 5, and 7 wt %)

Correspondence to: M. Kaci (kacimu@yahoo.fr).
Contract grant sponsor: EGIDE (TASSILI program).

prepared by melt extrusion are reported in this article.

EXPERIMENTAL

Materials used

PS used in this study in pellets form is an atactic homopolymer free of additives supplied by BASF Company under the trade name POLYSTYROL 143E. The material has an average M_w = 307,900 g/mol associated to a polydispersity index of 3.30, and a melt flow index of 10.43 g/10 min.

The type of nanofiller used is organophilic clay available from Southern Clay Product. It is commercialized under the trade name Cloisite 15 A. The Cloisite 15A is a montmorillonite OMMT modified by a quaternary ammonium salt, and dimethyl dehydrogenated tallow (2M2HT) with ~ 65% C18, 30% C16, 5% C14 and C.E.C. = 125 meq/100 g. The Cloisite 15A was used at various contents, i.e., 2.5, 5, and 7 wt %.

Preparation of PS/OMMT nanocomposites

The PS/OMMT nanocomposites were prepared by melt mixing in a Brabender Plasticorder mixing chamber (model W 50 EHT) having the following characteristics: chamber volume = 55 cm^3, sample weight = 40–70 g, maximum couple = 200 Nm and maximum temperature = 500°C. Prior mixing, the nanofiller was dried at 80°C for 24 h. The major processing parameters were processing temperature, screw speed and mixing time; they were set at 180°C, 50 rpm and 10 min, respectively. Using the same operating conditions, the neat PS was also processed for comparative purposes. The resulting extruded materials were granulated, and then compressed to produce thin films of an average thickness of ~ 150 μm with the aid of hydraulic press equipped with two heated plates at 200°C with a pressure of 20 bars. Different formulations based on PS were prepared with various clay contents: 0, 2.5, 5, and 7 wt %.

Accelerated UV test

Photo-oxydation was carried out on both PS and PS/OMMT nanocomposite films at $\lambda > 300$ nm by using a Sun Test (ATLAS) apparatus at a constant temperature of 40°C. This apparatus has been designed for the study of polymer photodegradation in artificial conditions corresponding to a medium acceleration of ageing. The apparatus consists of a Xenon lamp of 1500 Watt equipped with a cooling unit. The radiation is maintained at 270 W/m^2 in the interval 300–800 nm.[11] Both PS and PS/clay nanocomposite samples were subjected to various exposure times in the range: 24, 48, 72, 96, 120, 144, 192, and 216 h.

Characterization methods

Characterization of the nanocomposites

Wide angle X-ray scattering (WAXS). WAXS was used to analyze the structure of the nanocomposite materials and to determine the interlayer spacing between stacked clay platelets.[12] WAXS experiments were performed by using a Philips diffractometer (PW 1050) operating at the CuKα radiation (wavelength, λ = 0.154 nm), 40 kV and 20 mA. The diffraction spectra were recorded in the reflection mode over a 2θ range of 1–12° at room temperature and a scan rate of 0.017°/s.

Rheometry. Rheological measurements were carried out in an oscillatory mode on a rheometer (Gemini Bohlin, C-VOR), equipped with a parallel plate geometry using 25 mm diameter plates at 180°C. The samples in form of pellets having ~ 1 mm of thickness and 25 mm of diameter were prepared by compression molding at 180°C. The elastic modulus (G') was measured in the linear domain in a frequency range between 0.01 and 10 rad/s. The average time for scan measurement was 20 min.

Differential scanning calorimetry (DSC). Differential scanning calorimetry (DSC) analysis of both PS/OMMT nanocomposites and neat polymer was performed on weighted samples of almost 10 mg, using Mettler-Toledo DSC-882 equipment. The samples were heated from 25 to 200°C in nitrogen atmosphere. To erase thermal history, the first cooling and the second heating thermograms were recorded with the following scanning rate: 10°C/min in the first cooling and 10°C/min in the second heating.

Thermogravimetric analysis (TGA). TG experiments were carried out in a Setaram TG-DTA 92-10 thermal analyzer using a scanning rate of 10°C/min under nitrogen in the temperature range starting from 20 to 650°C.

Characterization of photo-oxidative degradation

Fourier transform infrared spectroscopy (FTIR). The chemical changes due to UV light were monitored by fourier transform infrared spectroscopy (FTIR) spectroscopy. The IR spectra were recorded using a PerkinElmer FTIR spectrometer with 2 cm^{-1} resolution and 40 scans. All spectra were recorded in the absorbance mode in the 4000–600 cm^{-1} region. The oxidation degree, i.e., carbonyl index under photo-oxidation was obtained by calculating the carbonyl absorption at 1725 cm^{-1} from the FTIR spectra at

different exposure times, using the spectrum of the starting unoxidized materials as reference. All measured absorbances were normalized by the film thickness according to the following eq. (1):[13]

$$\text{Carbonyl index} = [A_{1725}/d] \times 100 \quad (1)$$

where A_{1725} is the measured absorbance at 1725 cm^{-1} from the FTIR spectrum at certain exposure time, and d is the film thickness in microns.

Viscosimetric measurements. Viscosimetric measurements were made using an Ubbelhode solution viscosimeter at room temperature with toluene as solvent.[14,15] The kinetic energy and shear corrections were negligible. The Huggins equation was applied to estimate the intrinsic viscosity [η], which is related to the viscosity average M_w, M_v, by the Mark-Houwink-Sakurada equation, $[\eta] = K.M_v^a$ where K and a are empirical constants ($K = 4.16 \times 10^{-3}$ g/cm^3 and $a = 0.79$).[16] As a result of the polymer chain scission, [η] decreases with increasing the average number of random scissions per original polymer molecules.[15] The kinetics of photolysis were followed viscosimetrically using single point measurements for calculating limiting viscosity numbers.

Scanning electron microscopy (SEM). Morphologies were observed with a Jeol JSM-6031 scanning electron microscope (SEM) to examine the fractured surface of the nanocomposite samples. Before observation, the fractured surfaces of the specimen were coated with a thin gold layer by means of a polaron sputtering apparatus.

RESULTS AND DISCUSSION

Characterization of the samples

Wide angle X-ray scattering (WAXS) analysis

WAXS analysis was employed to quantify the gallery height between adjacent silicate platelets, and subsequently to prove the widening of this distance as matrix polymer intercalates between the galleries. Changes in the value of 2θ reflect changes in the gallery distance of the clay and allow distinguishing the intercalated and nonintercalated silicate fractions.[1,17] Accordingly, Figure 1 shows the diffraction patterns for neat PS, pristine OMMT and PS/OMMT nanocomposites prepared with various clay contents, i.e., 2.5, 5, and 7 wt %. As expected, no peak is observed in the WAXS pattern of neat PS (diffractogram 1), whereas in diffractogram 2 the pristine OMMT exhibits a sharp peak (d_{001}) at around 2.80°, corresponding to an interlayer *d*-spacing of 3.1 nm based on the Bragg's equation.

In X-ray diffraction curves of 2.5, 5, and 7 wt % PS/OMMT nanocomposites corresponding to diffractograms 3, 4 and 5, respectively, it is clearly

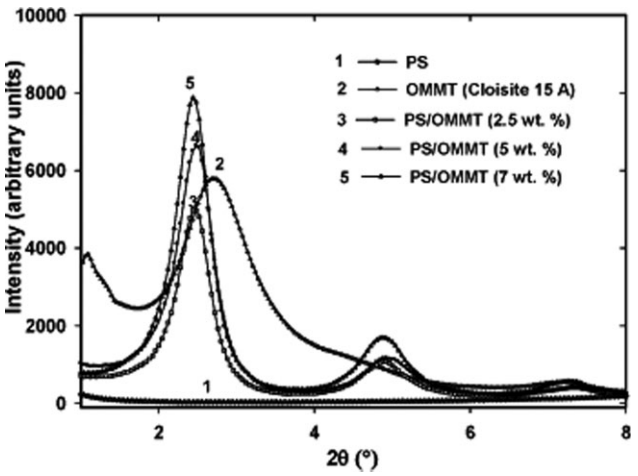

Figure 1 WAXD patterns of neat PS, OMMT, PS/OMMT (2.5 wt %), PS/OMMT (5 wt %), and PS/OMMT (7 wt %) nanocomposites.

observed that the (001) base peak position shifts into smaller angles passing from 2.80° for the pristine OMMT to 2.42° for the nanocomposites. This corresponds to an increase of the interlayer *d*-spacing of 3.65 nm for the PS/OMMT nanocomposites compared with 3.1 nm for OMMT. Moreover, the d_{001} peak is sharper and its intensity seems to increase slightly with the clay content. According to Tiwari and al.,[18] this result is attributed to the formation of intercalated nanocomposites without disruption of the multilayered order of clay layers. The authors reported also that more orientation order among clay layers occurs likely at higher loadings.

Furthermore, the increase in the *d*-spacing suggests the formation of intercalated layered silicate nanocomposites and hence good compatibility between the organophilic clay and PS.[8,19–21] However, it is noted that the WAXS patterns of the nanocomposite samples exhibit also the presence of a broad peak of less intensity, which is positioned at higher angle at $2\theta \approx 5°$. According to Jang et al.,[22] this result indicates that probably a small amount of clay was not well mixed with the polymer matrix. To further confirm the intercalation structure in the PS/OMMT systems, the measurement of rheological behaviors of the nanocomposite samples as compared with the neat polymer was performed.

Rheological measurement

One of the most convenient methods to elucidate the state of dispersion of polymer clay nanocomposites is linear viscoelastic characterization. Such experiments are expected to provide some information on the inner microstructures of the nanocomposites, such as the state of dispersion of clay and the confinement effect of silicate layers on the motion of polymer chains.[23–27] In this respect, the storage

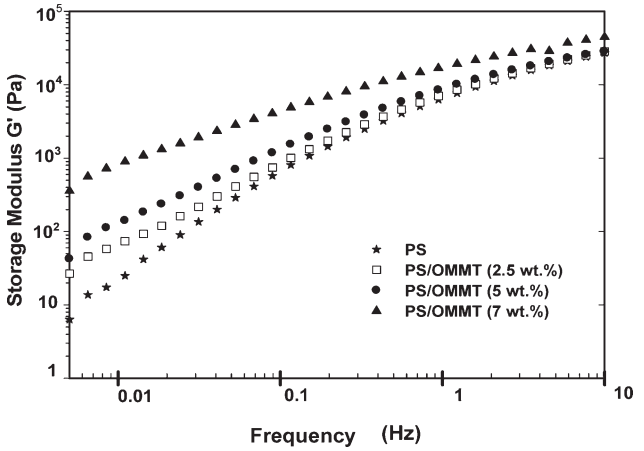

Figure 2 Storage modulus (G') of neat PS and PS/OMMT nanocomposites at various clay contents: 2.5, 5, and 7 wt % at 180°C.

modulus (G') resulting from the dynamic frequency scan measurements for neat PS and PS/OMMT nanocomposites with various clay loadings is compared in Figure 2. The curves show that the storage modulus of nanocomposite samples is substantially higher than that of neat PS. On the other hand, the slopes of G' seem to be lower for all the nanocomposite samples, especially for the PS/OMMT (7 wt %) compared to that of neat PS. Moreover, it is observed a regular increase in the magnitude of G' with the OMMT content at low frequencies. However, at high frequencies, G' of all the sample melts come nearer. The increase of G' is attributed to the reinforcing effects of OMMT layers/tactoids and associated to the results previously obtained using WAXS. This may also be an indication of the formation of partially intercalated structure of the PS/OMMT nanocomposites.[26,28] Generally, the contribution of intercalated clay to G' of the nanocomposites can be analyzed in terms of two effects—the confinement effect and the interparticle interactions, which result in the enhancement of low frequencies G' in comparison with the polymer matrix.[23,29]

Thermogravimetric (TGA) analysis

Figure 3 shows the TGA thermograms for both PS and PS/OMMT nanocomposites with various clay contents, i.e., 2.5, 5, and 7 wt %. As shown in Figure 3, the thermal stability of the whole PS/OMMT nanocomposites is significantly improved when compared with that of neat PS. Indeed, all the nanocomposite samples exhibit higher decomposition temperature than the polymer matrix, which seems to increase with the clay loadings. The analysis of TGA data at 50% weight loss indicates that the decomposition temperature value increases from 433°C for the neat PS to 447°C for PS/OMMT (2.5 wt %), 452°C for PS/OMMT (5 wt %) and 455°C for PS/OMMT (7 wt %). Furthermore, all the nanocomposites have a lower thermal degradation rate than that of neat PS. As reported in literature,[9,30,31] the clay brought up the thermal stability of PS significantly and this enhancement can be regarded as additional evidence of the intercalations between PS and OMMT. The OMMT has high thermal stability, and its layer structure exhibits a great barrier effect, which hinders the evaporation of the small molecules generated in the thermal decomposition process. This limits the continuous decomposition of the PS.

Differential scanning calorimetry (DSC)

Figure 4 shows the DSC thermograms for neat PS and PS/OMMT nanocomposites with various clay contents, i.e., 2.5, 5, and 7 wt %. Thermogram 1 indicates that the neat PS exhibits an endothermic

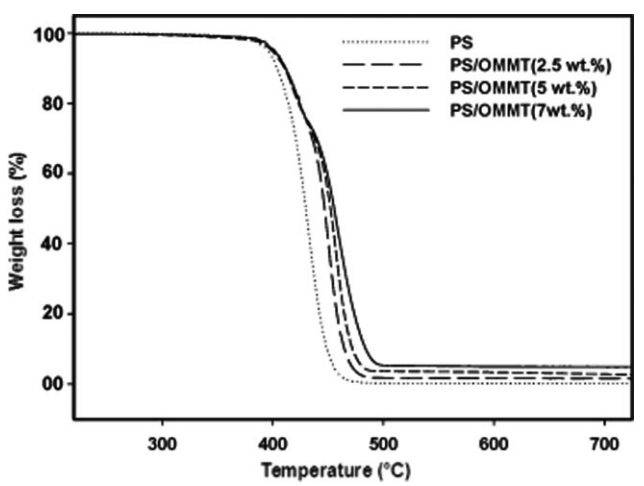

Figure 3 TGA thermograms of neat PS and PS/OMMT nanocomposites at various clay contents: 2.5, 5, and 7 wt %.

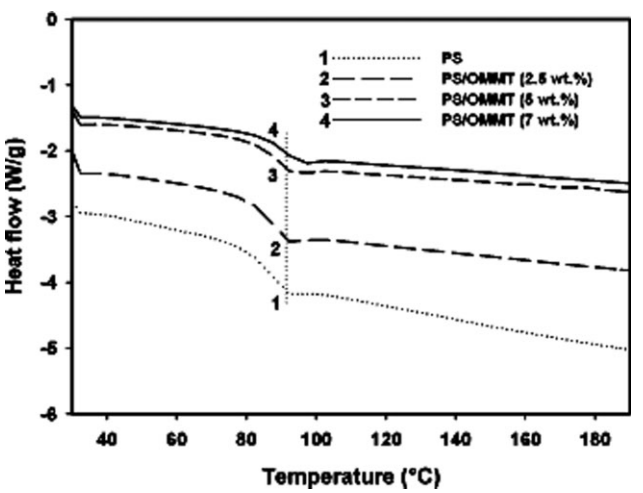

Figure 4 DSC thermograms of neat PS and PS/OMMT nanocomposites at various clay contents: 2.5, 5, and 7 wt %.

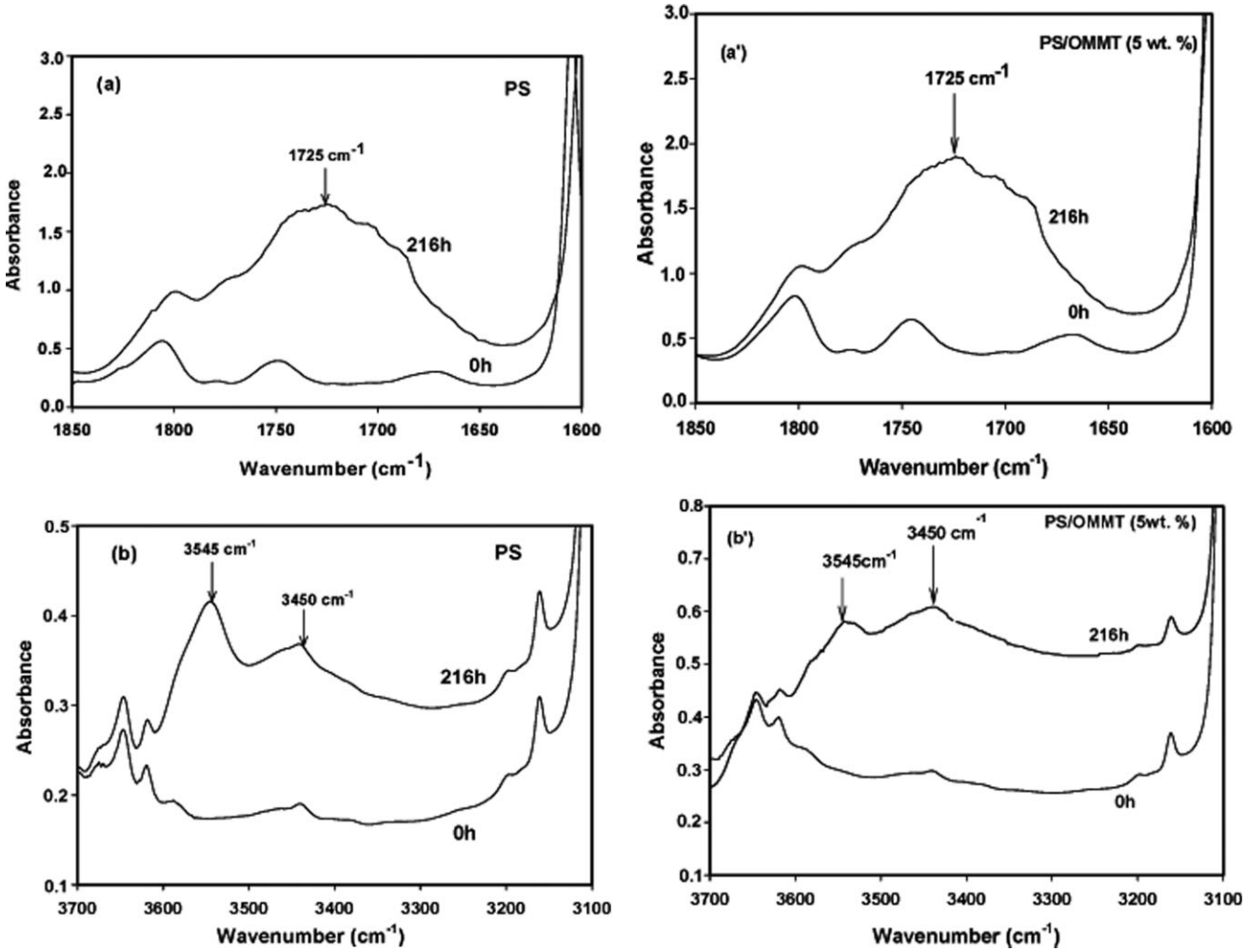

Figure 5 FTIR spectra for both neat PS and PS/OMMT (5 wt %) samples recorded before exposure and after 216 h in the carbonyl region: (a) PS and (a′) PS/OMMT (5 wt %) and the hydroxyl region (b) PS and (b′) PS/OMMT (5 wt %).

process centered at the temperature of almost 86°C, which corresponds to the glass-transition temperature (T_g) of the polymer. Moreover, it is observed in thermogram 2 and 3 that an increase in clay content to 5 wt % in PS nanocomposites seems to have no effect on T_g, which remains unchanged based on the neat PS. However, with further increase of the clay content to 7 wt %, a slight shift of T_g toward 89°C is noted as clearly shown in thermogram 4. According to the literature,[17,21] the increased T_g results from the restricted segmental motions of the polymer chains at the organic-inorganic interface, due to the confinement of the PS chains between the silicate layers, as well as the silicate surface polymer interaction in the nanostructured hybrids.

Accelerated photo-oxidation of PS/OMMT nanocomposites

Infrared analysis

As expected, the FTIR spectra of irradiated films of both neat PS and PS/OMMT nanocomposites with various clay contents, i.e., 2.5, 5, and 7 wt % exhibit significant modifications with respect to the initial films in the carbonyl (1850–1600 cm^{-1}) and hydroxyl (3600–3100 cm^{-1}) regions, but much more pronounced in the nanocomposite samples. The FTIR spectra of neat PS and PS/OMMT nanocomposite samples exhibit similar shape before and after UV exposure. This is clearly shown in Figure 5(a,a′), relative to the carbonyl region of PS and PS/OMMT (5%), respectively, and also, in Figure 5(b,b′) corresponding to the hydroxyl region. Moreover, the comparison of the different FTIR spectra of the nanocomposite samples with neat PS reveals also no displacement of the absorption band position in the presence of clay. In contrast, a rapid growth in the carbonyl and hydroxyl band intensity is observed with increasing exposure time for the nanocomposite samples in comparison with the polymer matrix; however this increase seems to be less affected by clay loadings. Furthermore, the analysis of FTIR spectra in Figure 5(a,a′) of neat PS and PS/OMMT (5%), respectively, taken as examples, indicates that

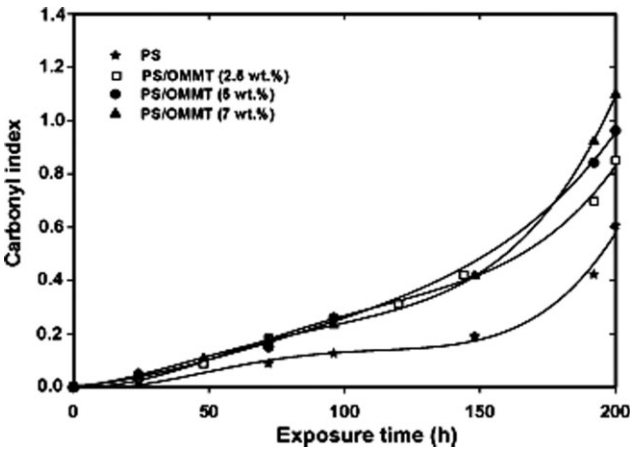

Figure 6 Carbonyl index versus exposure time for neat PS and PS/OMMT nanocomposites at various clay contents: 2.5, 5, and 7 wt %.

after 216 h of exposure, ketonic groups represent the main products resulting from the photo-oxidation process, and they are detected at $\lambda_{max} = 1725$ cm^{-1}. Besides this, the presence of shoulders at 1689, 1698, 1703, and 1710 cm^{-1} is also observed that correspond to probably acetophenone and aromatic end chain ketones, benzoic acid, benzaldehyde, and aliphatic acid, respectively. These photoproducts have also been identified previously.[17,32] In the hydroxyl region illustrated in Figure 5(b,b′), the degraded samples show a broad band peaking up at 3450 cm^{-1} attributed to hydroperoxide groups. A narrow band with a high intensity is also noticed with a maximum absorption band centered at 3545 cm^{-1} corresponding to alcohols (free hydroxyl groups).[33] The results above suggest that the photo-oxidation mechanism of the polymer matrix is not modified in presence of OMMT clay, but only the photo-oxydation rates are affected, confirming the data previously reported in literature.[4]

Figures 6 and 7 compare the photo-oxidation rates of both PS and PS/OMMT nanocomposites with various clay loadings, i.e., 2.5, 5, and 7 wt % through the changes of carbonyl index and absorbance at 3450 cm^{-1} with exposure time. As shown in Figure 6, it is observed that the induction time, which is associated to the resistance of material against oxidation, is higher for neat PS ($\approx$ 25 h), while it is shortened to almost 10 h for nanocomposite samples. Moreover, one can see clearly that after the induction period, the curve of carbonyl index versus time shows a sharp increase with a slope related to the rate of autooxidation. Accordingly, the carbonyl index evolution of PS/OMMT nanocomposites is much faster than that of neat PS. However, it is noted that the variation of the clay content has less effect on the photo-oxidation rate. Figure 7 shows the changes of the absorbance at 3450 cm^{-1} for both neat PS and PS/OMMT nanocomposites during UV irradiation. The same conclusions as above can be drawn, with the same peculiar behavior of PS/OMMT nanocomposites.

Viscosimetric measurements

The degree of degradation of both neat PS and PS/OMMT nanocomposites with various clay amounts is estimated from the number of main-chain scission index (SI) (or number of scissions per molecule). SI is defined according to the following eq. (2):[7,34,35]

$$\begin{aligned} \mathrm{SI} &= [n(t) - n(t_0)]/n(t_0) = [M_n(t_0)/M_n(t)] - 1 \\ &\approx [M_v(t_0)/M_v(t)] - 1 \end{aligned} \quad (2)$$

in which $n(t)$ represents the number of polymer chains at time t and $n(t_0)$ the initial number of chains, while $M_v(t_0)$ and $M_v(t)$ are the viscosity average M_w of samples before and after photo-oxidation, respectively. Figure 8 shows overall changes in the SI of PS/OMMT nanocomposites compared with pure PS as a function of exposure time. It is clearly observed that in neat PS, the SI curve increases slowly, but regularly during all the exposure time, whereas in nanocomposite samples, the curves have higher SI values, especially when the exposure time is above 50 h. The lower SI values determined for neat PS films indicate that much less chain scission takes place in the polymer when compared with PS/OMMT nanocomposite samples. Although the SI curves of the nanocomposites show a similar trend, however the addition of more OMMT to the PS matrix seems to produce a slight change in the SI values. Furthermore, it is observed that the scission rate of the neat polymer decreases in the final stage of degradation (above 200 h of UV exposure). In fact, this behavior is different from that observed with

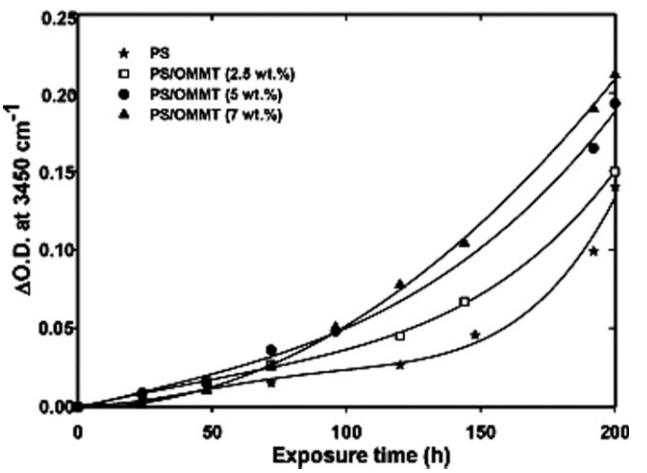

Figure 7 Variation of absorbance at 3450 cm^{-1} as a function of exposure time for neat PS and PS/OMMT nanocomposites at various clay contents: 2.5, 5, and 7 wt %.

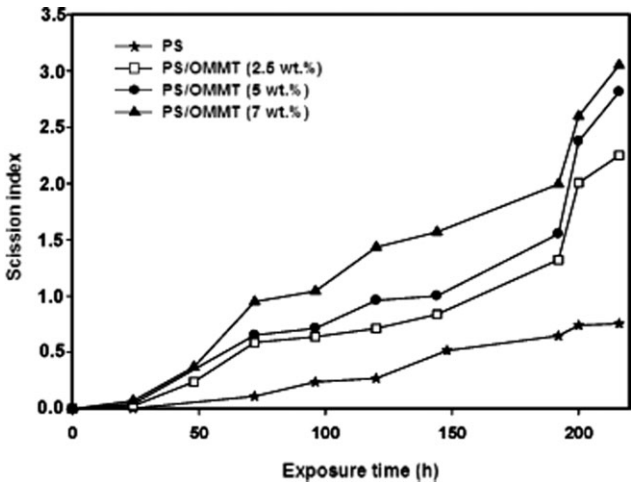

Figure 8 Scission index evolution versus exposure time for neat PS and PS/OMMT nanocomposites at various clay contents: 2.5, 5, and 7 wt %.

the same samples analyzed by FTIR spectroscopy (Figs. 6 and 7). The difference between the carbonyl index, which grows fast towards the end of degradation and the scission speed which declines, may result from the formation of oxidative species of very low M_w that cannot undergo the scission process. The presence of OMMT causes also an increase in the extent of PS degradation, which is relatively common when mineral fillers are added to polymers. The presence of free metallic ions in the clay act as catalyst to polymer. However, some authors[36] reported that this catalytic effect is reduced when the clay is organically modified.

Scanning electron microscopy (SEM)

The fractured surface of pure PS before and after 192 h of exposure was analyzed by SEM micrographs, as shown in Figure 9(a,b), respectively, at magnification of 2000. As shown in Figure 9(a), the micrograph of pure PS shows the fracture of a homogeneous material, but the appearance of different planes of fracture surface is indicating changes in the crack path during fracture. However after 192 h, the irradiated specimen exhibits a severe damage

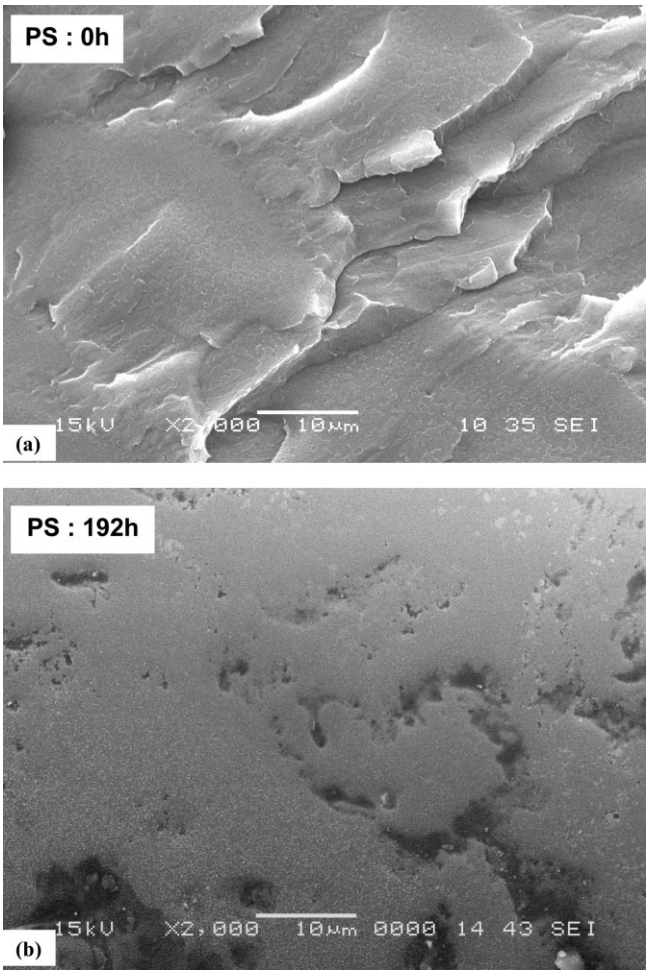

Figure 9 SEM micrographs of fractured surface for neat PS. (a) before irradiation (0 h) and (b) after 192 h of exposure.

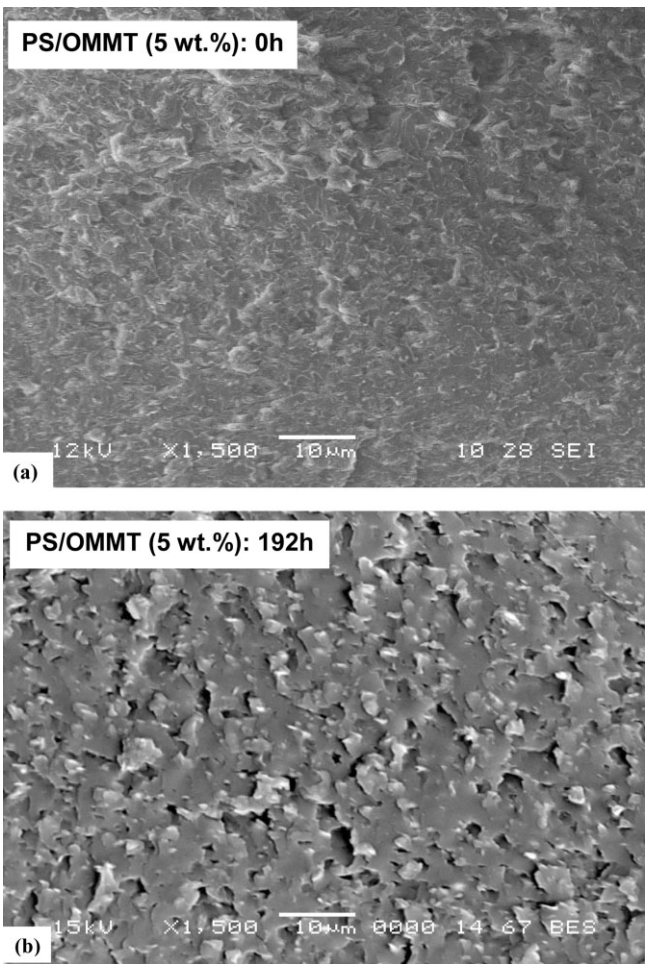

Figure 10 SEM micrographs of fractured surface for PS/OMMT (5 wt %). (a) before irradiation (0 h) and (b) after 192 h of exposure.

through surface erosion as a result of photo-oxidative degradation [Fig. 9(b)]. In fact, many holes of large area are clearly apparent on the irradiated surface. Figure 10(a,b) shows, as an example, the micrograph of the fractured surface of PS/OMMT nanocomposites containing 5 wt % of clay before exposure and after 192 h at a magnification of 1500. In Figure 10(a), the fractured surface of the nanocomposite sample is characterized by the presence of small domains homogeneously distributed associated with a large dispersion of particle sizes. After 192 h [see Fig. 10(b)], the fractured surface shows the presence of a high number of microvoids of different dimensions. The damage resulted from degradation is almost the same as that noted for the other formulations.[29]

CONCLUSIONS

PS/OMMT nanocomposites have been prepared with various clay loadings, i.e., 2.5, 5, and 7 wt % by melt processing. Both WAXS analysis and rheological measurements confirm the expansion of the clay layers associated with intercalation. Moreover, the TGA and DSC analyses indicate that the thermal stability of PS/OMMT nanocomposites becomes higher than neat PS.

The effect of accelerated photo-oxidation on the structure, M_w and morphology of PS/OMMT nanocomposites has been studied up to 216 h of exposure as a function of clay loading, using FTIR spectroscopy, viscosimetry and SEM, respectively. The study reveals that the degradation rate of PS/OMMT nanocomposites is higher than the pure polymer, which is attributed to the catalytic behavior of the clay. On the other hand, the variation of clay content is found to have less influence on the photo-oxidative degradation of the nanocomposite materials. Furthermore, the photodegradation mechanism of both PS and PS/OMMT nanocomposites proceeds mainly through chain scission as evidenced by a large increase of both the carbonyl index and the SI. Additionally, the SEM micrographs of the fractured surfaces of the degraded materials exhibit eroded surfaces.

References

1. Wagener, R.; Reisinger, T. J. G. Polymer 2003, 44, 7513.
2. Burmistr, M. V.; Sukhyy, K. M.; Shilov, V. V.; Pissis, P.; Spanoudaki, A.; Sukha, I. V.; Tomilo, V. I.; Gomza, Y. P. Polymer 2005, 46, 12226.
3. Pandey, J. K.; Raghunatha Reddy, K.; Pratheep Kumar, A.; Singh, R. P. Polym Degrad Stab 2005, 88, 234.
4. Leroux, F.; Meddar, L.; Mailhot, B.; Morlat-Thérias, S.; Gardette, J. L. Polymer 2005, 46, 3571.
5. Qin, H.; Zang, S.; Liu, H.; Xie, S.; Yang, M.; Shen, D. Polymer 2005, 46, 3149.
6. Singh, R. P.; Vishwa Prasad, A.; Solanky, S. S. J Appl Polym Sci 2002, 85, 1676.
7. Bottino, F. A.; Cinquegrani, A. R.; Di Pasquale, G.; Leonardi, L.; Orestano, A.; Pollicino, A. Polym Test 2004, 23, 779.
8. Chigwada, G.; Wang, D.; Wilkie, C. A. Polym Degrad Stab 2006, 91, 848.
9. Li, H.; Yu, Y.; Yang, Y. Eur Polym J 2005, 41, 2016.
10. Kizilkaya, O.; Ono, M.; Morikawa, E. J Elect Spect Relat Phenom 2006, 151, 34.
11. Kaci, M.; Hebal, G.; Touati, N.; Rabouhi, A.; Zaidi, L.; Djidjelli, H. Macromol Mater Eng 2004, 289, 681.
12. Rohlmann, C. O.; Failla, M. D.; Quinzani, L. M. Polymer 2006, 47, 7795.
13. Sampers, J. Polym Degrad Stab 2002, 76, 455.
14. Hardlovič, P.; Lukáč, I.; Zvara, I.; Kuličková, M.; Berek, D. Eur Polym J 1980, 16, 651.
15. Chee, K. K. Polym Degrad Stab 1996, 52, 45.
16. Matsuo, T.; Inagaki, H. Makromol Chem 1962, 53, 130.
17. Yei, D. R.; Kuo, S. W.; Fu, H. K.; Chang, F. C. Polymer 2005, 46, 741.
18. Tiwari, R. R.; Khilar, K. C.; Natarajan, U. J Appl Polym Sci 2008, 108, 1818.
19. Wu, T. M.; Hsu, S. F.; Wu, J. Y. J Polym Sci Part B: Polym Phys 2002, 40, 736.
20. Dazhu, C.; Haiyang, Y.; Pingsheng, H.; Weian, Z. Comp Sci Technol 2005, 65, 1593.
21. Uthirakumar, P.; Song, M.-K.; Nah, C.; Lee, Y.-S. Eur Polym J 2005, 41, 211.
22. Jang, B. N.; Wilkie, C. A. Polymer 2005, 46, 9702.
23. Li, J.; Zhou, C.; Wang, G.; Zhao, D. J Appl Polym Sci 2003, 89, 3609.
24. Zhong, Y.; Zhu, Z.; Wang, S. Q. Polymer 2005, 46, 3006.
25. Bartholome, C.; Beyou, E.; Bourgeat-Lami, E.; Cassagnau, P.; Chaumont, P.; David, L.; Zydowicz, N. Polymer 2005, 46, 9965.
26. Ding, C.; Guo, B.; He, H.; Jia, D.; Hong, H. Eur Polym J 2005, 41, 1781.
27. Tanoue, S.; Utracki, L. A.; Garcia-Rejon, A.; Sammut, P.; Ton-That, M. T.; Pesneau, I.; Kamal, M. R.; Lyngaae-Jørgensen, J. Polym Eng Sci 2004, 44, 1061.
28. Hoffmann, B.; Dietrich, C.; Thomann, R.; Friedrich, C.; Mülhaupt, R. Macromol Rapid Commun 2000, 21, 57.
29. Touati, N.; Kaci, M.; Ahouari, H.; Bruzaud, S.; Grohens, Y. Macromol Mater Eng 2007, 292, 1271.
30. Kim, T. H.; Lim, S. T.; Lee, C. H.; Choi, H. J.; Jhon, M. S. J Appl Polym Sci 2003, 87, 2106.
31. Zhang, W. A.; Shen, X. F.; Liu, M. F.; Fang, Y. E. J Appl Polym Sci 2003, 90, 1692.
32. Mailhot, B.; Jarroux, N.; Gardette, J. L. Polym Degrad Stab 2000, 68, 321.
33. Duarte, F. M.; Botelho, G.; Machado, A. V. Polym Test 2006, 25, 91.
34. Weir, N. A.; Whiting, K. Eur Polym J 1989, 25, 291.
35. Shyichuk, A. V. J Appl Polym Sci 1996, 62, 1735.
36. Ramos Filho, F. G.; Mélo, T. J. A.; Rabello, M. S.; Silva, S. M. L. Polym Degrad Stab 2005, 89, 383.